1-2012

Development of a Digital Fringe Projection Technique to Characterize the Transient Behavior of Wind - Driven D roplet/Rivulet Flows

Bin Wang
Iowa State University

William F. Lohry
Iowa State University, wflohry@iastate.edu

Song Zhang
Iowa State University, song@iastate.edu

Hui Hu
Iowa State University, huhui@iastate.edu

Development of a Digital Fringe Projection Technique to Characterize the Transient Behavior of Wind - Driven D roplet/Rivulet Flows

Abstract
Thin film flows naturally arise in a wide variety of industrial and environmental problems ranging from microchip manufacturing, structured packing to lava flows in geology. In particular, wind-driven flows of liquid films are of great interests for deeper understanding of aircraft icing and better design of anti-icing and de-icing strategies. Currently, most thickness mapping techniques involves complicated experimental layout and expensive measuring facilities, for example, photo-luminescence, and stereoscopic techniques. In this study, we successfully applied Fourier transform profilometry for the thickness measurement of wind-driven droplet flows. This technique has been very popular in many fields, like 3D sensing, object recognition, but less known in the fluid dynamics community. It features simple experimental layout, low cost, high spatial resolution, and real time thickness measurement. All these merits motivate us to explore wider and better application of this technique and its variants in the field of fluid mechanics.

Keywords
Aerospace Engineering

Disciplines
Aerodynamics and Fluid Mechanics | Graphics and Human Computer Interfaces | Manufacturing

Comments
This is a conference proceeding from *50th AIAA Aerospace Sciences Meeting* (2012): 1, doi:10.2514/6.2012-261. Posted with permission.

50th AIAA Aerospace Sciences Meeting including the New Horizons Forum and Aerospace Exposition
09 - 12 January 2012, Nashville, Tennessee

AIAA 2012-0261

Development of a Digital Fringe Projection Technique to Characterize the Transient Behavior of Wind-Driven Droplet/Rivulet Flows

Bin Wang[1], William Lohry[2], Song Zhang[3] and Hui Hu[4](✉)

Iowa State University, Ames, Iowa, 50011

Abstract

Thin film flows naturally arise in a wide variety of industrial and environmental problems ranging from microchip manufacturing, structured packing to lava flows in geology. In particular, wind-driven flows of liquid films are of great interests for deeper understanding of aircraft icing and better design of anti-icing and de-icing strategies. Currently, most thickness mapping techniques involves complicated experimental layout and expensive measuring facilities, for example, photo-luminescence, and stereoscopic techniques. In this study, we successfully applied Fourier transform profilometry for the thickness measurement of wind-driven droplet flows. This technique has been very popular in many fields, like 3D sensing, object recognition, but less known in the fluid dynamics community. It features simple experimental layout, low cost, high spatial resolution, and real time thickness measurement. All these merits motivate us to explore wider and better application of this technique and its variants in the field of fluid mechanics.

1 Introduction

Thin film flows are of fundamental importance in various fields of human endeavor, including lava flows in geology, tertiary oil recovery, lubricant oil films in tribology, surface coating, printing and cleaning process, manufacturing and protection of microchips, biofilm transport within mammalian lungs, icing of the aircrafts and wind turbines, structured packing, and so on (Cazabat et al. 1990, Oron et al. 1997, Zhao et al 2006). Despites all the importance and mysteriousness of thin film flows, current understandings on them are still limited due to their intrinsic complexity. In general, the thin film flows are characterized by the behaviors of the deformable interface between the base flow and the external environment (Cobelli et al. 2009). Various physical effects, like, viscous, surface-tension, body forces, thermo-capillarity, evaporation/condensation, long-range molecular forces (e.g. van der Waals forces), surface curvature/roughness, etc, may all contribute to the thin film free surface deformations at varied extents under different circumstances (Oron et al. 1997). Numerous theoretical and numerical investigations have been conducted to enhance the understandings of the underlying physical mechanisms of thin film flows germane to specific interests of different research groups (Zhao et al 2006). Nevertheless, both theoretical predictions and numerical analysis still need to survive the tests of carefully controlled experiment through a suitable measurement technique.

[1] Graduate Student, Department of Aerospace Engineering.
[2] Undergraduate Graduate Student, Department of Chemical and Biological Engineering.
[3] Assistant Professor, Department of Mechanical Engineering.
[4] Associate Professor, Department of Aerospace Engineering, AIAA Associate Fellow, Email: huhui@iastate.edu

Experimental works have been reported for fingering instability associated with thin film flows, spinning drops (Huppert 1982, Melo et al. 1989, Cazabat et al. 1990, de Bruyn 1992, Fraysse & Homsy 1994, Hocking et al. 1999, Ward 2009), and wind-driven rivulet breakoff and droplet flows in microgravity and terrestrial-gravity conditions (McAlister et al. 2005). But all these results are based on snapshots of the propagating contact lines, thus precise film thickness information cannot be obtained. With the continued advances of flow visualization techniques, the thickness field of the thin film flow can be directly mapped to facilitate further in-depth analysis of the physical phenomena. Liu et al. (1995) used fluorescent imaging method to measure the dynamic relative film thickness variation due to the three-dimensional (3D) instability of gravity-driven film flows. Later, Johnson et al (1997, 1999) also developed a fluorescent imaging system for the purpose of studying gravity-driven film flows. They verified their system by measuring flow phenomena germane to several broad areas including wave phenomena on a continuous film, fluid rupture behavior, and rivulet shapes. Fluorescence intensity-based approach was later reported to be used to measure film thickness in different engineering contexts (Lel et al 2005, Chinnov et al. 2007, Schagen et al. 2007). Variants of this technique were also found in the literature (Carlos et al. 2001).

Also, density-based approaches, stereoscopic techniques, and single point measurement methods have been successfully applied to the measurement of free surface deformations. Zhang el al. (1996) developed a density-based color light encoding technique to measure free-surface gradients, and successfully applied this technique to the mapping of surface deformation due to near-surface turbulence. Other density-based approaches include the diffusing light photography (Wright et al. 1996), qualitative optical Schlieren techniques (Kabov et al. 2002), and the quantitative free-surface synthetic Schlieren (FS-SS) method (Moisy et al. 2007). In addition, stereoscopic techniques have also been successfully exploited to measure the 3D sea wave elevations (Benetazzo 2006), and unsteady dam break flows (Eaket et al. 2005). A remarkable feature of this method is its capability to measure surface discontinuities (Tsubaki et al. 2005). Single point thickness tracking was also found in the literature. Recently, Zhang et al. used capacitance-based thickness metering system to investigate the surface waves riding on the heated falling liquid film (2009).

Another large category of 3D deformable shape measurement technique is the method of structured light projection. This technique relies on a projector-like functional block to actively project coded light patterns on the object, and extracts the 3D object shape from the distorted images of the light patterns captured from a different perspective (Salvi et al. 2004). It has been applied very successful in many fields including 3D sensing, object recognition, robot control, industrial inspection of manufactured parts, reverse engineering, stress/strain and vibration measurements, biometrics, biomedicine, dressmaking, visual media and so on. Actually, this technique is attracting increasing attention in the fluid dynamics community as well. Cazabat et al. (1990) observed the climbing film driven by temperature gradients using reflection microscope, and mentioned that equally spaced fringes were used to reconstruct the thickness profiles of thin spreading films. Grant et al. (1990) employed the projection moiré method to measure water waves in study of the wave-structure interactions for the safe and cost-effective design of offshore structures, and they used wave probes to resolve the ambiguity associated with the determination of peak or trough of the fringes.

With the advances in digital display technology, the fringes typically used in a structured light projection system can be directly generated by the digital projectors rather than through Ronchi gratings as used in the projection moiré method. This digital adaptation to the measurement system further

simplifies the set-up and enables higher measurement accuracy due to the precise control of the fringe patterns. Zhang and Su (2002) applied this digital fringe projection technique to the reconstruction of the vortex shape at a free surface, and they used the Fourier-transform algorithm to extract the vortex shape from images of the deformed fringes. This method is commonly known as Fourier transform profilometry (FTP) (Taketa et al. 1982, 1983) in the field of optical 3D non-contract profilometry for solid surfaces. Almost at the same time, Pouliquen et al. (2002) employed similar method to record the time evolution of the free surface deformations of dense granular flow. More recently, Cochard et al. (2008) designed a digital fringe projection system to measure the time-evolution of the surge down an inclined plate due to the dam break. Cobelli et al. (2009) demonstrated the successful measurement of water waves using their digital fringe projection system as well.

In order to further our understanding of wind-driven flows, a FTP-based digital fringe projection system with high spatial and temporal resolution is carefully designed to measure the free surface deformations of the wind-driven droplets. The reason this technique is selected for the experiment is that it offers good measurement accuracy with low cost and simple set-up. This effort is innovative in several aspects. First of all, defocused binary fringes are used instead of the conventional focused sinusoidal fringes (Zhang 2010). This adjustment allows for further simplification of the system set-up and opens up opportunities for high frequency applications. Also, many technical problems associated with this particular application need to be sorted out before taking any data with confidence.

2 Principle of the method

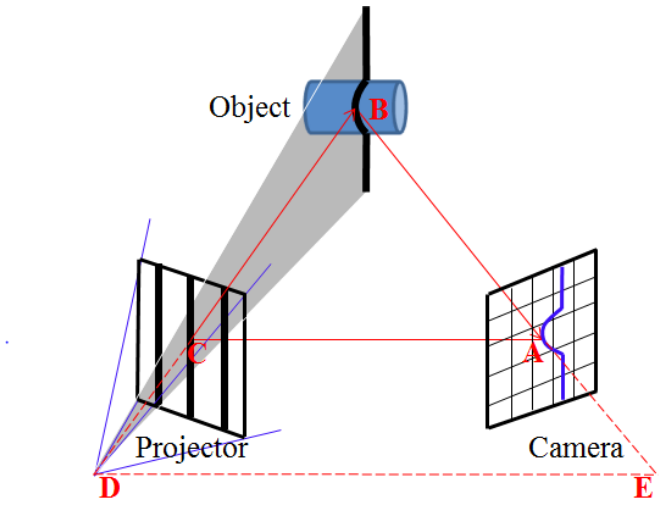

Fig. 1 Schematic representation of the digital fringe projection system

2.1 Digital fringe projection system set-up

The majority of the fringe projection systems are based on the principle of structured light triangulation in similar manner as the stereo vision system but replacing one of the two cameras in the latter system with a projector-like device as shown in Fig. 1. In other words, in a typical fringe projection system, the projection unit (D), image acquisition unit (E), and the 3D object (B) form a triangulation base. If the correspondence between the camera pixel (A) and the projector pixel (C) is identified, the depth information at point B can be recovered through the triangulation (△ABC). Specifically, the projector

projects a fringe pattern of known characteristics onto the test object, and due to the 3D geometrical profile of the object, the fringe pattern is deformed seen from a perspective different from the projection axis. Usually, the fringe pattern on a reference plane is recorded by the same system. By comparing between the distorted fringe pattern over the object and the reference fringe pattern, the 3D profile of the object with respect to the reference plane can be retrieved. In a word, the object geometry is actually encoded in the phase difference between the deformed and reference fringe images.

2.2 Fourier Transform method

Among all possible fringe patterns, the binary and sinusoidal fringes are extensively used in the fringe projection system. Binary-coded structured patterns have the merits of easy implementation and robust to noise. But the spatial resolution achieved using binary patterns is limited by the pixel representation of the projector. As a comparison, the sinusoidal fringes can have varying intensity values from pixel to pixel. With proper interpolation techniques, sub-pixel level spatial resolution can be achieved (Zhang 2010). Most recently, Zhang et al. (2010) proposed a flexible 3D shape measurement technique using the defocused binary patterns (DBP). Compared with the focused sinusoidal patterns (FSP), the DBP method does not require precise synchronization between the projector and the camera, and the correction of the projector's nonlinear gamma effect becomes unnecessary. These flexibilities further simplify the experimental procedures without considerably compromising the accuracy and also open up new opportunities for high speed applications. Therefore, the DBP method is used in the experiment.

The intensity of the defocused binary fringe pattern recorded by the camera can generally be expressed as multiple signals with spatial carrier frequencies n/p modulated in both phase $\phi(x,y,t)$ and amplitude $A(x,y,t)$, as given by the following Fourier series expansion

$$I(x,y,t) = \sum_{n=-\infty}^{\infty} q_n(x,y,t)\, exp(j2\pi ny/p) \tag{1}$$

Where

$$q_n(x,y,t) = A_n(x,y,t) exp[jn\phi(x,y,t)] \tag{2}$$

where $A_n(x,y,t)$represents unwanted amplitude modulation due to the light source and inhomogeneous surface reflectivity of the test object, the phase $\phi(x,y,t)$contains the desired shape information of the 3D object, p is the fringe pitch on the reference plane. Also, it is worth to be noted that zero frequency intensity value corresponds to the undesirable background intensity variation over the field of view. Since the phase carries information about the 3D shape to be measured, the strategy would be to separate the phase $\phi(x,y,t)$ out from the intensity signal.

By using discrete Fourier Transform in spatial domain, the Fourier spectra of the intensity $I(x,y,t)$ distribution captured at a certain instant can be obtained. Since in most cases $A_n(x,y,t)$and $\phi(x,y,t)$vary very slowly compared with the spatial frequency of the fringe given by$1/p$, all the spectra are well separated from each other. We can do filtering operation to single out the spectrum of the fundamental frequency component, and compute its inverse Fourier transform to obtain a complex signal as written below

$$\hat{I}(x,y,t) = A_1(x,y,t)exp\{j[2\pi y/p + \phi(x,y,t)]\} \quad (3)$$

The same signal processing can be done for the reference fringe images to obtain

$$\hat{I}_0(x,y) = \mathcal{A}(x,y)exp\{j[2\pi y/p + \phi_0(x,y)]\} \quad (4)$$

Then the phase difference can be calculated from a new signal as given below

$$\hat{I}(x,y,t) \cdot \hat{I}_0^*(x,y) = A_1(x,y,t)\mathcal{A}(x,y)exp\{j[\Delta\phi(x,y,t)]\} \quad (5)$$

where $*$ indicates complex conjugate of the signal, and $\Delta\phi(x,y,t) = \phi(x,y,t) - \phi_0(x,y)$ is the phase difference between the deformed fringes over the object and the reference fringes. And it is usually computed from the ratio between the imaginary and real part of the new signal as written below

$$\Delta\phi(x,y,t) = arctan\{Im[\hat{I}(x,y,t) \cdot \hat{I}_0^*(x,y)]/Re[\hat{I}(x,y,t) \cdot \hat{I}_0^*(x,y)]\} \quad (6)$$

It might be noted that the phase distribution calculated from the arctangent function is wrapped in the range$[-\pi,\pi]$, thus the nonphysical phase jumps have to be removed using reliable phase-unwrapping algorithms. This topic is in itself a vast research area, and it is not our intention here to dig into the details, but rather point the keen readers towards the informative book by Ghiglia et al. (1998).

2.3 Phase-to-height conversion

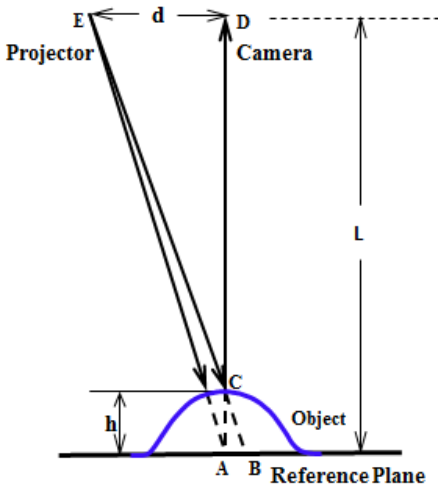

Fig. 2 Schematic diagram for phase-to-height conversion

Figure 2 illustrates the optical configuration of the measurement system and the phase-to-height conversion mechanism. The optical axis of the camera is perpendicular to the substrate (x-y plane) in the z direction, and the camera and projector are chosen to be arranged in the crossed-optical-axes geometry. As the name explains itself, the optical axis of the projector crosses the optical axis of the camera at point A on the reference plane (x-y plane). This optical set-up is easy to construct compared with the parallel-optical-axes geometry, and the phase modulation on the fringes due to the non-telecentric projector optics

can be automatically corrected in FTP. For more details regarding this issue, the readers are referred to the seminal work by Takeda (1983).

As shown in Fig. 2, the center of the entrance pupil of the camera lens is denoted by D, and the center of the exit pupil of the project lens is indicated by E. These two pupils are located at the same height l and separated by a distance d. Suppose that there is no object on the reference plane, ray EB from the projector will hit on point B on the substrate, as displayed. Due to the three-dimensional shape of the object, in this case, the light ray EB is intercepted at point C by the object. From the perspective of the camera, the image patterns have changed from the signal encoded on EA to that on EB after the object is put into the view of the camera. And this pattern shift is resulted from the height change h from point A to point C. Following this line of thought, the height h at some point of the object should be able to be retrieved from the pattern shift $\overline{AB}$.

Mathematically, this height conversion concept can be formulated as follows. Noting that ΔABC is geometrically similar to ΔDEC, we can write

$$\overline{AB} = dh(x, y, t)/[L - h(x, y, t)] \tag{7}$$

It follows that

$$h = \frac{\overline{AB}\, L}{\overline{AB} + d} \tag{8}$$

If the maximum height of the object is much smaller than the distance between the camera/projector and the reference plane, namely, $h \ll L$, the above equation can be linearized (Zhang et al. 2002), and reduced to a simplified form

$$h = \frac{L}{d}\,\overline{AB} \tag{9}$$

3. Experimental apparatus and procedures

Figure 3 illustrates the complete digital fringe projection system developed for the study of wind-driven droplet flows. One remarkable feature is the simplicity of the system layout as mentioned before. A laptop is used to control the projector and the camera. Dell LED projector (M109S) equipped with lens with F/2.0 and f=16.67mm is used to project the stationary defocused binary fringe images. The fringe images are captured by the Imaging Source digital universal serial bus CCD camera (DMK 21BU04) with a Computar M3514-MP lens (F/1.4, f=35mm). The camera has a maximum frame rate of 60 frames/s with a resolution of 640×480. The exposure time of the camera is set at 1ms. The projector has a resolution of 858×600.

A Plexiglas test section with the dimension of $20 \times 14 \times 30\ cm$ $(W \times H \times L)$is built to study the free surface deformation of the wind-driven droplet flows. The maximum achievable wind speed of the wind tunnel is roughly 35m/s. In order to obtain fringe images with high contrast, the surface of the object to be measured is required to have high diffuse reflectivity. Unfortunately, the mirror-like surface of water makes it more likely to have specular reflection than diffuse reflection. Therefore, heavy whipping cream is used to demonstrate the viability of the system for the study of wind-driven droplet flows. To further

remove the specular highlights at the interface, polarizers are placed in front of the projector and the camera. And it is found that polarization can improve the image quality for reflective surfaces such as liquids without deteriorating the projected fringe patterns though the background intensity reduces. For future work, we might consider adding certain white liquid dye to the water to enhance its diffuse reflectivity but not to affect its hydrodynamic properties like viscosity and surface tension (Cobelli 2009).

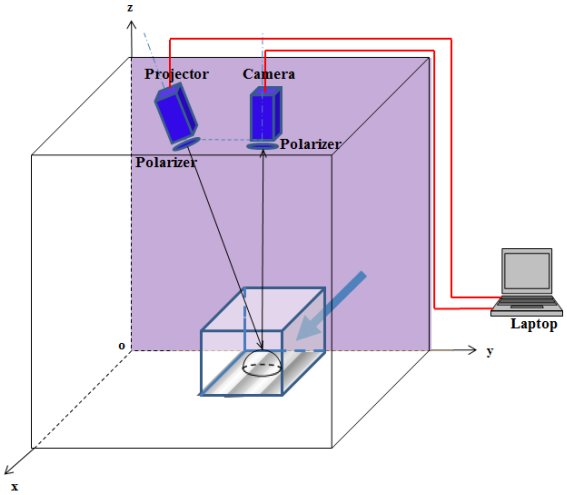

Fig. 3 Layout of the digital fringe projection system developed for the study of wind-driven droplet flows

4. System calibration and verification

The mapping from the pattern shift to the physical height is obtained based on the linear conversion approximation as discussed in section 2.3. The calibration result is displayed in Fig. 4 (a). As can be seen from the figure, linear approximation is reasonably valid in the measurement range, and the phase-to-height conversion coefficient is found to be 1.0266 mm/radians in this case. After the calibration, the accuracy of the system can be tested using an object with known characteristics (Zhang et al. 2010). A tiny frustum of pyramid with 5mm height, 15 × 15mm base and 45-degree slopes at four sides are printed using an in-house 3D plastic printer. To improve the diffuse reflectivity of the surface, the test object is coated with flat white paint.

The selection of the fringe pitch is a trade-off between competing demands of high spatial resolution and good image quality. Thus, the optimal fringe pitch is usually determined case by case. Figure 4 (b) reveals typical deformed fringe image for a flat-top pyramid using the FTP-based system; the wrapped phase map obtained from the Fourier transform based algorithm is displayed in Fig. 4(c); and the corresponding height distribution of the object is shown in Fig. 4 (d). Note that Gaussian filter is used to smooth out the high order noise from the raw results. Also, measurement errors are calculated from the absolute difference between the designed shape of the object and the measured height distribution. While Fig. 5(a) shows the quantitative comparison between the true height of the pyramid and the measurement results of the pyramid height, Fig. 5 shows the distributions of the measurement errors within the measurement window. It can been seen that relatively large errors usually occur at the boundaries due to the shadow effect and texture change from the substrate to the object. The root-mean-square of the measurement errors in the measurement window was found to be about 0.16mm for the present study. It should be noted that the measurement uncertainties due to the manufacturing errors of the test object are not taken into account at this point.

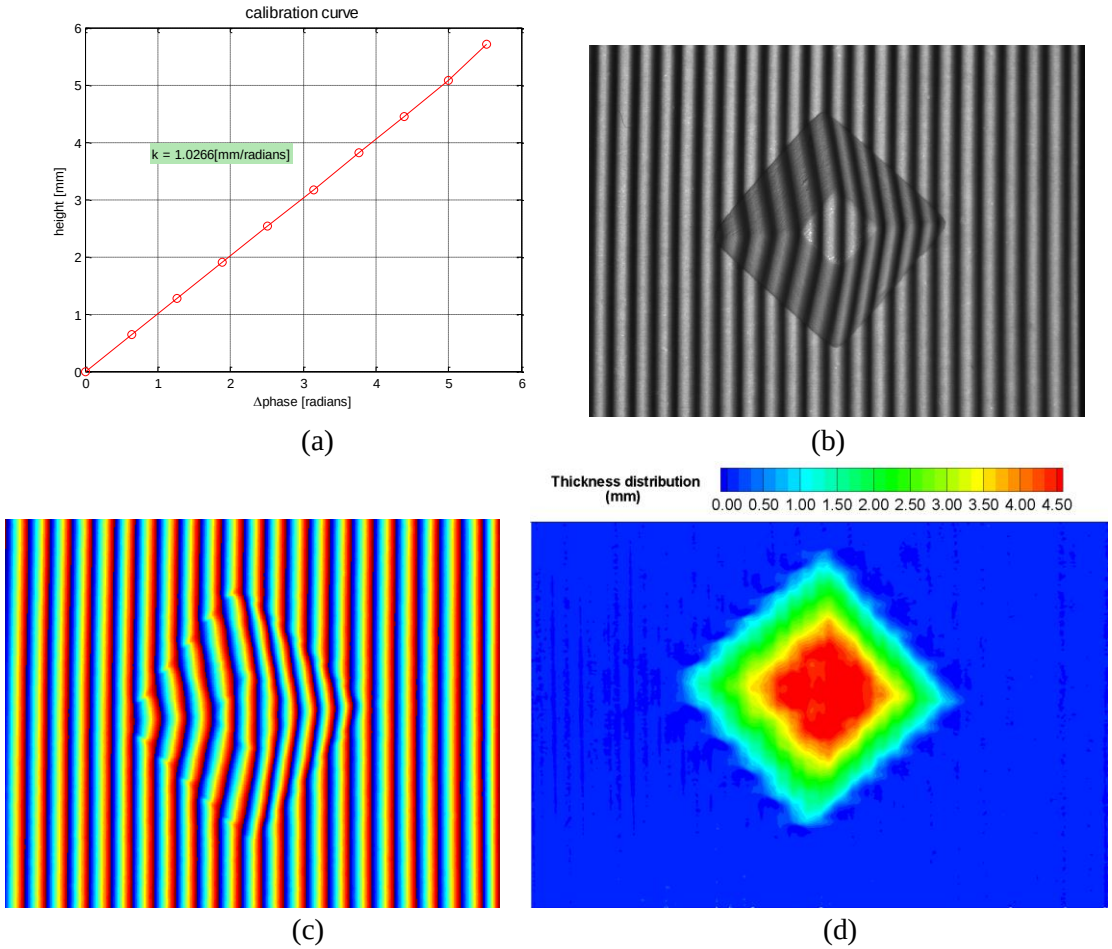

Fig. 4 Measurement results of a flat-top pyramid using the FTP-based system. (a) Calibration curve. The phase-to-height conversion coefficient k is 1.0266 mm/radian in this case. (b) Typical deformed fringe images over the object. (c) Wrapped phase map of the object. (d) Height reconstruction of the object.

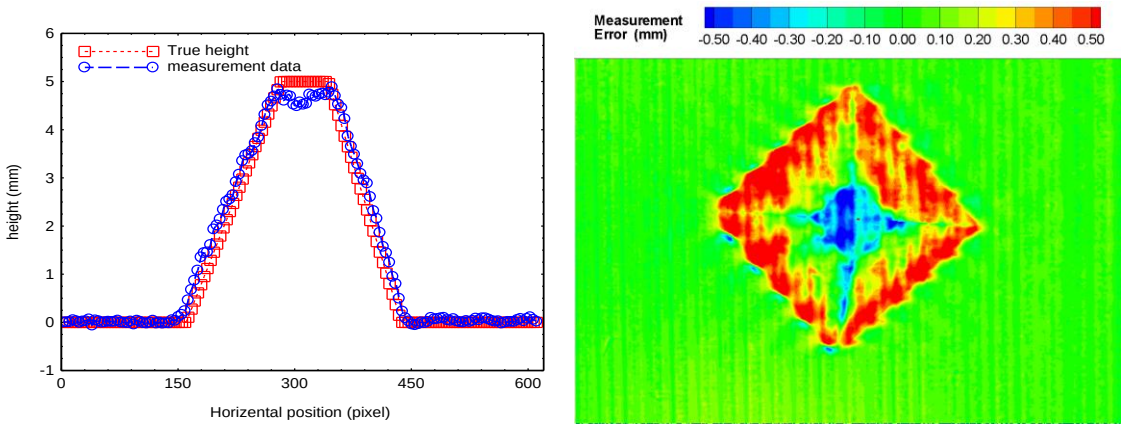

Fig. 5: (a).Quantitative comparison between the true height of the pyramid and the measured value along a horizontal line; (b) Measure error distribution in the measurement window.

5 Demonstrations

In this section, the performance of the developed digital fringe projection system is illustrated with experimental examples showing its capability of capturing wind-driven droplet flows. Fig. 6 shows typical raw images of the transient wind-driven droplet flows at different instants, and Fig. 7 are the corresponding post-processed results. The contours indicate the thickness of the thin films. Note that the contact lines of the droplets are not accurately detected by the current algorithm due to the shadow effect and texture change near the edges. In future work, windowed Fourier transform method might be implemented to improve the measurement accuracy near the boundary (Qian 2004).

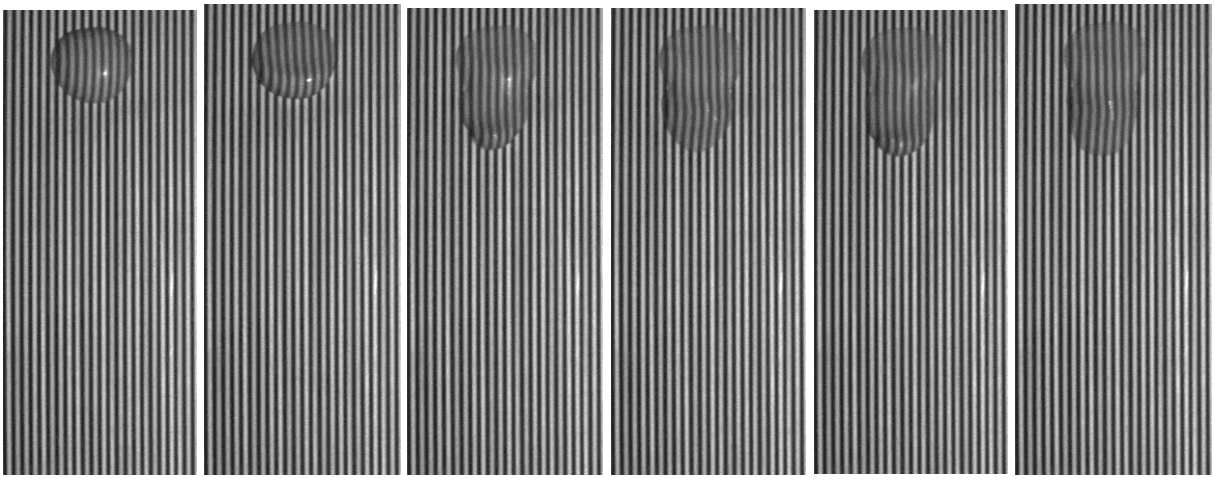

(a) (b) (c) (d) (e) (f)

Fig.6 Deformed fringe images of the transient droplet flows captured by the developed digital fringe projection system at increasingly time instants.

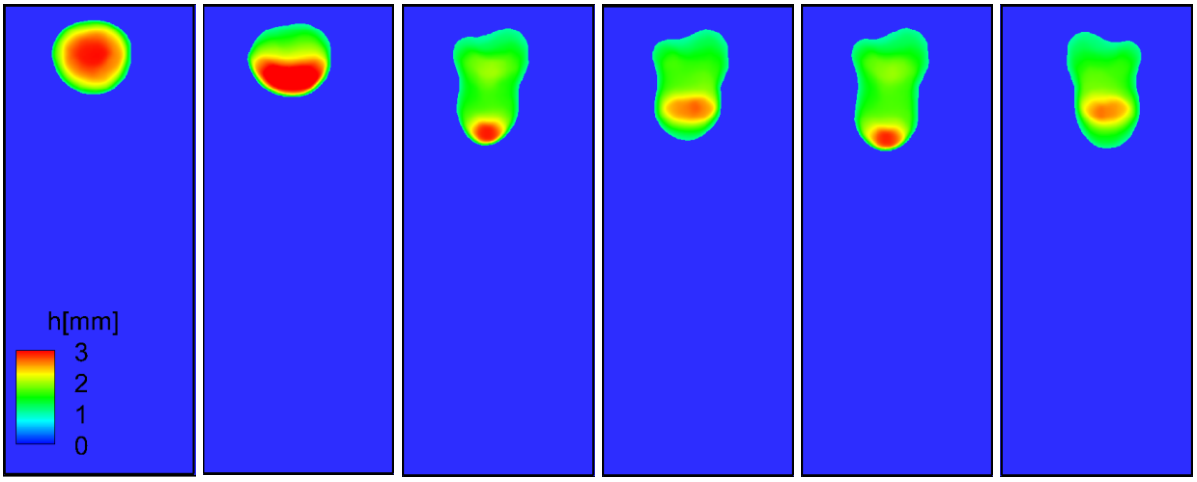

(a) (b) (c) (d) (e) (f)

Fig.7 Post-processed results of the transient droplet flows shown in Fig. 6. The contour levels are based on the film thickness h with unit mm.

As displayed above, the droplet propagates driven by the wind, and deforms due to the free surface waves. It is observed in the experiments that the dynamics of droplet flows can be influenced by a variety

of controlling parameters, for example, wind speed, droplet size, contact line shape, hydrodynamic properties of the droplet, substrate properties, and so on.

As the droplet moves downstream, a tail of the droplet leaves behind the propagating droplet head as shown above. For relatively thin fluid, it is observed that droplet detachment frequently happen. However, In this case, the head of the droplet is not seen detached from the 'mother' drop, probably due to the relatively high viscosity of the testing fluid. For future research, the hydrodynamic properties of the testing fluid will be matched with water to provide insights into the possible flow regimes of wind-driven water droplet flows. Interestingly, it is found that when the front lobe of the droplet is not energetic enough to push forward the contact lines, the fluid is transported from the front lobe to the rear section, then sloshes back to the front lobe, and finally overcomes the surface tension and lurches forward. This observation is similar to the "inchworm motion" reported by McAlister et al. (2005), though the controlled experimental conditions are different in our case compared with theirs. Further detailed study and modeling work might be able to shed light on this phenomenon.

6 Conclusions

In order to provide insights into the wind-driven droplet flows, a new fringe projection based measurement system is set up and tested on objects of known shape with good measurement accuracy. Three-dimensional droplet-thickness profiles are measured in real time with high spatial resolution using the developed system to demonstrate its applicability. The current system features simple set up, low cost, high spatial and temporal resolution, and good measurement accuracy. In future work, windowed Fourier transform method will be implemented to improve the measurement accuracy near the contact lines. Also, it would be of interest to investigate possible flow regimes of wind-driven droplet flows in dominating non-dimensional parameter space using the developed fringe projection based measurement system.

References

Benetazzo A(2006) Measurements of short water waves using stereo matched image sequences. Coastal Engineering 53(12):1013-1032

Cazabat AM, Heslot F, Troian SM, Carles P(1990) Fingering instability of thin spreading films driven by temperature gradients.Nature 346: 824 -826

Carlos HH, Douglas PH(2001) Emission reabsorption laser induced fluorescence (ERLIF) film thickness measurement. Meas. Sci. Technol. 12(14):467-477

Chinnov E, Kharlamov S, Saprykina A, Zhukovskaya O(2007) Measuring deformations of the heated liquid film by the fluorescence method. Thermophysics and Aeromechanics 14(2):241-246

Cobelli PJ, Maurel A, Pagneux V, Petitjeans P(2009) Global measurement of water waves by Fourier transform profilometry. Exp Fluids 46:1037-1047

Cochard S, Ancey C(2008) Tracking the free surface of time-dependent flows: image processing for the dam-break problem. Exp Fluids. 44:59-71

de Bruyn JR(1992) Growth of fingers at a driven three-phase contact line. Phys. Rev. A 46: R4500–R4503

Eaket J, Hicks FE, Peterson AE(2005) Use of Stereoscopy for Dam Break Flow Measurement. J. Hydr. Engrg. 131(1):24-29

Fraysse N, Homsy GM(1994) An experimental study of rivulet instabilities in centrifugal spin coating of viscous Newtonian and non-Newtonian fluids. Phys. Fluids 6: 1491–1504

Ghiglia DC, Pritt MD(1998) Two-dimensional phase unwrapping: theory, algorithms, and software. Wiley-Interscience, Wiley,cop.

Grant I, Stewart N, Padilla-Perez IA(1990) Topographical measurements of water waves using the projection moire method. Appl. Opt. 29(28):3981-3983

Hocking LM, Debler WR, Cook KE (1999)The growth of leading-edge distortions on a viscous sheet. Phys. Fluids 11: 307–131

Huppert HE(1982) Flow and instability of a viscous current down a slope. Nature 300: 427–429

Johnson MFG, Schluter RA, Bankoff SG(1997) Fluorescent imaging system for global measurement of liquid film thickness and dynamic contact angle in free surface flows. Rev. Sci. Instrum. 68(11):4097-4102

Johnson MFG., Schluter RA, Miksis MJ, Bankoff SG(1999) Experimental study of rivulet formation on an inclined plate by fluorescent imaging. J. Fluid Mech. 394: 339–354

Kabov OA, Scheid B, Sharina IA, Legros J(2002) Heat transfer and rivulet structures formation in a falling thin liquid film locally heated. International Journal of Thermal Sciences 41(7):664-672

Lei S, Zhang S(2010) Digital sinusoidal fringe pattern generation: Defocusing binary patterns VS focusing sinusoidal patterns. Optics and Lasers in Engineering 48(5):561-569

Lel V, Al-Sibai F, Leefken A, Renz U(2005) Local thickness and wave velocity measurement of wavy films with a chromatic confocal imaging method and a fluorescence intensity technique Exp. Fluids 39(5):856-864

Liu J, Schneider JB, Gollub JP(1995) Three-dimensional instabilities of film flows. Phys. Fluids 7(1): 55-67

McAlister G, Ettema R, Marshall JS(2005) Wind-driven rivulet breakoff and droplet flows in microgravity and terrestrial-gravity conditions. J.Fluids Engineering 127: 257-266

Melo F, Joanny JF, Fauve S(1989) Fingering instability of spinning drops. Phys. Rev. Lett.63: 1958–1961

Moisy F, Rabaud M, Salsac K. (2009) A synthetic Schlieren method for the measurement of the topography of a liquid interface. Exp. in Fluids 46 (6), 1021-1036.

Oron A, Davis SH, Bankoff SG(1997) Long-scale evolution of thin liquid films. Rev. Mod. Phys. 69(3):931-980

Pouliquen O, Forterre Y(2002) Friction law for dense granular flow: application to the motion of a mass down a rough inclined plane. J. Fluid Mech. 453:133-151

Qian K (2004) Windowed Fourier transform for fringe pattern analysis. Applied Optics. 43(13): 2695-2702.

Salvi J, Pagès J, Batlle J(2004) Pattern Codification Strategies in Structured Light Systems. Pattern Recognition 37:827-849

Schagen A, Modigell M(2007) Local film thickness and temperature distribution measurement in wavy liquid films with a laser-induced luminescence technique. Exp. Fluids 43:209-221

Takeda M, Ina H, Kobayashi S(1982) Fourier-transform method of fringe-pattern analysis for computer-based topography and interferometry. J. Opt. Soc. Am. 72(1):156-160

Takeda M, Mutoh K(1983) Fourier transform profilometry for the automatic measurement of 3-D object shapes. Appl. Opt. 22(24):3977-3982

Tsubaki R, Fujita I(2005) Stereoscopic measurement of a fluctuating free surface with discontinuities. Meas. Sci. Technol.16(10):1894-1902

Ward T, Wey C, Glidden R, Hosoi AE, Bertozzi AL(2009) Experimental study of gravitation effects in the flow of a particle-laden thin film on an inclined plane. Phys. Fluids.21(8):083305

Wright WB, Budakian R, Putterman SJ(1996) Diffusing Light Photography of Fully Developed Isotropic Ripple Turbulence. Phys. Rev. Lett.76(24):4528-4531

Zhang C, Huang PS, Chiang F(2002) Microscopic Phase-Shifting Profilometry Based on Digital Micromirror Device Technology. Appl. Opt.41(28):5896-5904

Zhang F, Peng J, Geng J, Wang Z, Zhang Z(2009) Thermal imaging study on the surface wave of heated falling liquid films. Experimental Thermal and Fluid Science 33(3):424-430

Zhang Q, Su X(2002) An optical measurement of vortex shape at a free surface. Optics & Laser Technology. 34(2):107-113

Zhang S, Van Der Weide D, Oliver J(2010) Superfast phase-shifting method for 3-D shape measurement. Optics Express 18(9):9684-9689

Zhang S(2010) High-resolution, high-speed 3-D dynamically deformable shape measurement using digital fringe projection techniques. Book chapter in: Advances in Measurement Systems

Zhang S(2010) Flexible 3D shape measurment using projector defocusing: extended measurement range. Optics letters 35(7):3080-3082

Zhang X, Dabiri D, Gharib M(1996) Optical mapping of fluid density interfaces: Concepts and implementations. Rev. Sci. Instrum.67 (5):1858-1868

Zhao Y, Marshall JS(2006) Dynamics of driven liquid films on heterogeneous surfaces. J. Fluid Mech. 559:355-378